Batteries & Supercaps

Review
doi.org/10.1002/batt.202400551

Chemistry Europe
European Chemical Societies Publishing

www.batteries-supercaps.org

Bulk Alloy Anodes for Sodium-Ion Batteries

Xiaohan Wang,[a] Xiaoying Zhao,[a] and Liubin Wang*[a, b]

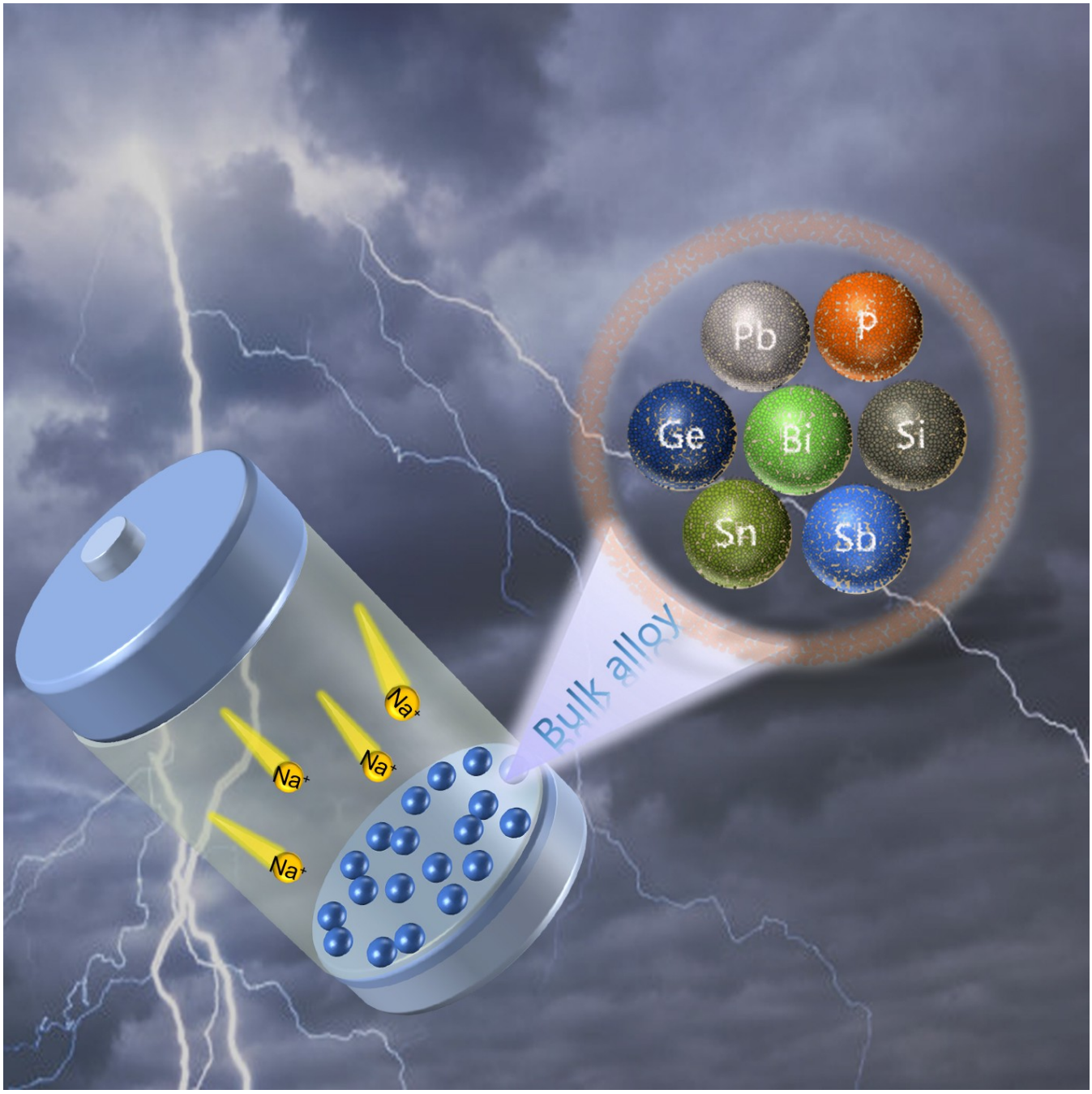

Sodium-ion batteries (SIBs) are considered a promising candidate for next-generation energy storage systems due to the abundance of available sodium resources. The practical application of SIBs critically depends on developing durable electrode materials with high capacity and long lifespan, particularly when it comes to finding suitable anode materials. Alloy-type anodes are appealing for their high capacities owing to the multiple electron transfer alloying reaction mechanism, making them ideal for high-energy-density SIBs. However, the huge volume change during charge/discharge process can cause the active material pulverization to detach from the current collector, leading to poor cycling performance, especially for bulk alloy anodes. Despite this challenge, recent progress in bulk or micro-sized alloy anodes for SIBs have shown promise. This review highlights the up-to-date advancements and research on bulk alloy-based anode materials for SIBs, including synthetic strategies and electrochemical performance. The crucial role of bulk alloy anodes in advancing SIB technology is discussed, along with a summary of research on bulk alloy-type anodes and their compounds for sodium storage. Strategies to improve the electrochemical performance of bulk alloy-based anode materials are also explored. Additionally, the potential of multi-component alloys and high-entropy alloys as future research directions for alloy-based anodes is proposed.

1. Introduction

Lithium-ion batteries (LIBs) have been widely used in portable electronic devices and electric vehicles due to their high energy density. However, the increasing demand of LIBs has led to the depletion of limited lithium resources and rising costs.[1–3] Sodium-ion batteries (SIBs) are seen as a promising alternative to addressing the shortcomings in the application of LIBs and regarded as an ideal choice for the next generation of large-scale energy storage technologies, as sodium resources are more abundant, wide distributed, and cost-effective.[4,5] Since Na and Li are in the same main group of the periodic table, the working mechanism of SIBs is similar to that of LIBs, i.e., "rocking chair" (Figure 1a).[6] During the charging and discharging process, Na^+ is embedded/de-embedded repeatedly between the cathode and anode. Although SIBs are similar to LIBs, the larger size of Na^+ (1.02 Å) compared to that of Li^+ (0.76 Å) and lower operating voltage (−2.71 V vs. SHE) present challenges in finding suitable and stable electrode materials and achieving high energy density in SIBs.[7,8] Improving the electrochemical performance of SIBs is crucial for the wide application of SIBs in large-scale energy storage. Electrode materials play a key role in battery performance, affecting cycle life, specific capacity, and operating voltage.[9,10] Stable electrode materials are essential to prevent side reactions with the electrolyte, maintain structural integrity, and inhibit pulverization and detachment of electrode materials. The search for suitable anode and cathode materials for SIBs is a pressing need.

Cathode materials for SIBs are typically characterized by high potential and specific capacity. Significant progress has been made in the development of cathode materials for SIBs, with a focus on various metal oxides (Na_xTMO_2, where $x \leq 1$ and TM represents metals like Mn, Fe, Co, Cu, etc.), polyanionic compounds ($Na_xM_y(X_aO_b)$, with M representing transition metals, X representing elements like P, S, Si, W, etc.), and Prussian blue analogs ($Na_xM_1[M_2(CN)_6]_{1-y}\cdot\square_y\cdot nH_2O$ with $0 \leq x \leq 2$ and $0 \leq y \leq 1$, where M_1 and M_2 denote distinct transition metal ions, such as Mn, Fe, Co, Ni, Cu, Zn, etc. and $\square$ represents vacant sites).[11–16] Some of these materials have demonstrated promising performance, with a few already in commercial production. Conversely, anode materials in SIBs hold the potential for achieving higher energy densities due to their diverse nature and high theoretical capacity.[17,18] Anodes are generally classified into three main types based on their charge storage mechanisms: insertion, conversion, and alloying.[19–22] Hard carbon, derived from biomass or organic precursors, is a commonly used insertion anode material in battery technology. However, its capacity is limited to less than 300 $mAh\,g^{-1}$.[23] Conversion anode materials comprising transition metal compounds like oxides, sulfides, selenides, and phosphides, offer higher specific capacity but face challenges related to low conductivity, voltage hysteresis, and high irreversible capacity.[24–27] Alloying-type reaction mechanism materials, derived from groups IVA (e.g., Si, Ge, Sn, Pb) and VA (e.g., P, Sb, Bi) of the periodic table, are highly regarded as promising anode materials due to their high theoretical capacity, good conductivity, suitable working potential, and cost-effectiveness (Figure 1b).[28,29] It has attracted a lot of interest from researchers and some progress has been made.[30,31] However, these alloy anodes undergo a multi-electron transfer alloying reaction mechanism, leading to significant volume changes and voltage fluctuations during charge/discharge. This can cause voltage hysteresis, inactivation of active materials, instability of the solid electrolyte interface (SEI), and ultimately affect cycling performance.[32,33] To address these challenges, nanomaterial design and hybridization with carbon or inert elements have been proposed to mitigate these issues, improving the discharge/charge process and minimizing volume effects. However, this approach may lead to a reduction in the overall energy density of the material, an increase in SEI formation, and a decrease in initial Coulombic efficiency (ICE).[34,35] In addition, the low tap density of nanostructures could impact the battery's bulk energy density. It is important to consider that well-designed nanomaterials necessitate intricate production processes, resulting in high manufacturing costs. In contrast, micro

[a] X. Wang, X. Zhao, L. Wang
College of Chemistry and Materials Science, Key Laboratory of Analytical Science and Technology of Hebei Province, Hebei Research Center of the Basic Discipline of Synthetic Chemistry, Hebei University, Baoding, Hebei 071002, P.R. China
E-mail: lbwang@hbu.edu.cn
[b] L. Wang
The Flame Retardant Material and Processing Technology Engineering Research Center of Hebei Province, Hebei University, Baoding, Hebei 071002, P.R. China

or bulk materials exhibit greater potential for practical applications across various aspects including volumetric energy density, Coulombic efficiency, manufacturing processes, and cost-effectiveness.[36,37] The advantages of micro or bulk alloy anodes include higher tap density, enabling increased mass loading and consequently enhancing volumetric capacity. Furthermore, the reduced specific surface area of these materials diminishes contact with the electrolyte, thereby improving the ICE in the first cycle. The simplicity of manufacturing processes and the resulting cost advantages render micro or bulk materials appealing for practical applications (Figure 2).

This review summarizes recent research progress on bulk phase and micro-sized alloy anode materials for SIBs, focusing on their advantages and challenges. Scientific issues concerning the development of bulk alloys of Bi, Sn, Sb, P, Si, Ge, and Pb are re-discussed, along with effective strategies to address these challenges, including electrolyte optimization, structural engineering, and multicomponent approaches to mitigate volume expansion and enhance electrochemical performance. Future directions and prospects for bulk phase alloy anode materials in SIBs are also explored, providing guidance for future research and commercial development aimed at advancing high-efficiency energy storage devices. We hope the deep insight into bulk alloy anode in SIBs could help us to understand and develop high-performance SIBs.

2. Bulk Alloy Anodes

Metals concentrated in groups IVA and VA of the periodic table, such as Bi, Sn, Sb, Pb, Ge, Si, and P, are capable of alloying/de-alloying reactions with Na, involving multi-electron transfer reactions to form alloying compounds (Na_xM, e.g., Na_3Bi, $Na_{15}Sn_4$, Na_3Sb, $Na_{15}Pb_4$, NaGe, NaSi, Na_3P). The reaction mechanism can be represented as: $xNa^+ + xe^- + M \rightarrow Na_xM$. Table 1 provides a summary of the discharge products, theoretical specific capacity, volume change upon complete sodium embedding, and voltage plateau of these alloyed anodes. Among them, Bi, known for its green and environmentally friendly nature, unique layered structure, and suitable working potential, exhibits a modest volume expansion (250%), enhancing rate capability and stability.[38,39] Sn offers a high theoretical specific capacity (847 $mAh\,g^{-1}$) and abundant resources but experiences significant volume expansion upon complete alloying to form $Na_{15}Sn_4$, impacting its electrochemical performance.[40,41] Sb, characterized by abundance and affordability, demonstrates a suitable working voltage and high theoretical specific capacity, leading to a high power density.[42] Furthermore, the amorphous state of Sb during sodiation enhances Na^+ diffusion kinetics, showing significant promise for advancement. Notable active phosphorus materials in element P include black phosphorus and red phosphorus.[43–45] Black P features good electrical conductivity, high specific capacity, and a distinctive layered structure, demonstrating excellent electrochemical performance in SIBs. However, its stability is lacking, and its preparation is intricate. In contrast, red P is straightforward and cost-effective to produce but suffers from poor electronic conductivity and substantial volume expansion during sodiation, limiting its practical utility in SIBs. The sodium-embedded mechanism of Pb resembles that of Sn, resulting in the formation of $Na_{15}Pb_4$ with a high theoretical specific capacity (485 $mAh\,g^{-1}$) and significant volume expansion (~375%).[46] In comparison to other alloy anode materials, Ge and Si exhibit smaller volume expansions of 205% and 114%, respectively.[47,48] However, they can only have certain Na-storage capacity in the amorphous state. The alloy anode material through an alloying reaction involving multiple electron transfers achieves a high specific capacity (> 300 $mAh\,g^{-1}$), along with a suitable working potential (0.2–

Xiaohan Wang received her B.S. degree from North China University of Science and Technology in 2022. She is currently a master student at Hebei University. Her main research interests are focused on high-performance electrode materials for sodium-ion batteries.

Xiaoying Zhao received her B.S. degree from Neijiang Normal University in 2021 and M.S. degree from Hebei University in 2024. Her current research interests are focused on functional nanomaterials and electrode materials in sodium-ion batteries.

Liubin Wang is a special-term Professor in the College of Chemistry and Materials Science, Hebei University. He obtained his B.E. degree in Materials Science and Engineering from Southwest Jiaotong University (2015) and Ph.D. degree in Physical Chemistry from Nankai University (2020). He worked as a visiting scholar at The University of Hong Kong in 2019. His research interests focuses on designing of electrodes and electrolyte for high-energy electrochemical devices, including metal-ion batteries, aqueous batteries, photo-assistant rechargeable batteries, etc.

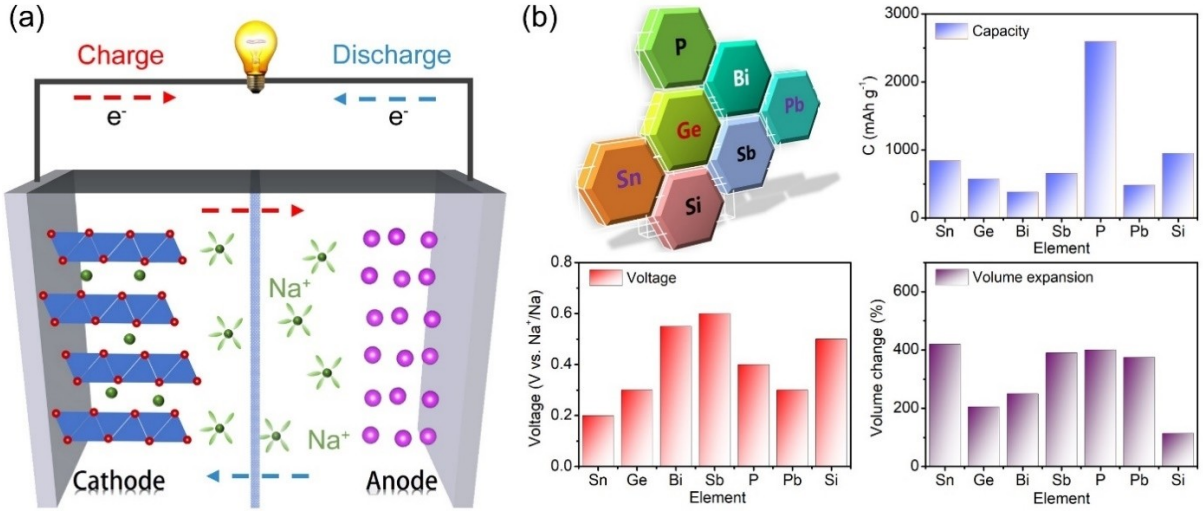

Figure 1. (a) Schematic illustration of the sodium storage mechanism in SIBs; (b)Theoretical capacity, voltage plateau, and volume expansion rate of Bi, Sn, Sb, P, Pb, Si, and Ge alloy anodes.

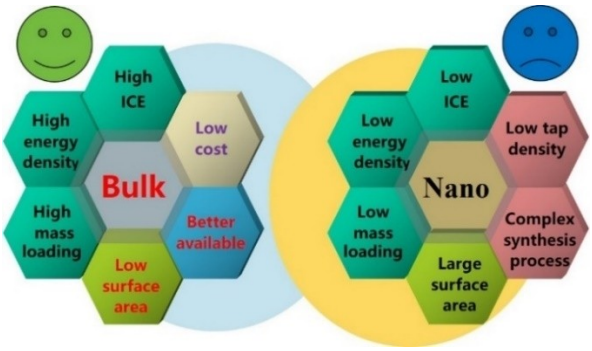

Figure 2. Comparison of micron-sized alloys and nanosized alloys.

0.6 V), high volumetric energy density, good electronic conductivity, and abundant reserves. This establishes them as potential candidates for anode materials in high-performance SIBs.[Table 2]

Although, alloyed anode materials show promising applications in electronic energy storage. However, they suffer from drawbacks such as high initial irreversible specific capacity, capacity degradation, and inadequate rate performance.[49,50] The sodium embedding/desorption process in these materials, particularly in its bulk phase, results in significant volume expansion due to the larger Na^+ radius, leading to electrode material structure fragmentation. This fragmentation exposes more interfaces, triggering persistent side reactions and sluggish kinetic responses, ultimately resulting in subpar cycling and multiplicity performance. These challenges have impeded practical implementation. Various strategies, including carbon coatings, special structure design, multicomponent alloy strategy, electrolyte optimization, architecture engineering, and binder selection, have been explored to address the limitations of bulk-phase alloy materials (Figure 3).[51–53] The objective of this study is to investigate the latest research developments on bulk alloy anodes and conduct a comprehensive analysis of these findings as reviewed according to different elements in the following sections.

2.1. Bismuth (Bi)

Metal Bi is a promising anode material for SIBs due to its ability to form Na_3Bi through sodium embedding, providing a theoretical specific capacity of 385 $mAh\,g^{-1}$, high ionic and electronic conductivity, and a unique lamellar structure with a large layer spacing (d (003) = 3.95 Å), as well as abundant and

Table 1. Summary parameters of alloy anodes for SIBs.

Type of Alloy	Final discharge product	Theoretical capacity ($mAh\,g^{-1}$)	Volume expansion (%)	Voltage platform (V vs. Na^+/Na)	Ref.
Bi	Na_3Bi	385	250	~0.55	[38]
Sn	$Na_{15}Sn_4$	847	420	~0.2	[40]
Sb	Na_3Sb	660	390	~0.6	[42]
P	Na_3P	2596	~400	~0.4	[44]
Pb	$Na_{15}Pb_4$	485	375	~0.2	[46]
Si	NaSi	954	114	~0.5	[47]
Ge	NaGe	576	205	~0.3	[48]

Table 2. Summary of different modification strategies to improve the electrochemical performance of bulk alloy anodes.

Materials	Synthetic method	Electrolyte	Cyclic performance ($mAh\,g^{-1}$/Cycle)	Current density ($mA\,g^{-1}$)	Rate performance ($mAh\,g^{-1}$/$mA\,g^{-1}$)	Ref.
Bulk Bi	Commercial	1 M $NaPF_6$ in diglyme	390.8/2000	2000	356.0/2000	[56]
Bi	Commercial	1 M $NaPF_6$ in diglyme	356/100	400	150/8000	[58]
Bi/C	One-pot carbonization	DME	270/1000	5000	280.35/10000	[59]
P–Bi/C	Sol-gel method	DME	178/20000	50000	153.2/60000	[60]
3DPB	Liquid phase reduction	1 M $NaPF_6$ in DME	374/3000	10000	378/10000	[61]
FBi@NC	Hydrothermal	1 M $NaPF_6$ in DME	261.4/10000	5000	368.2/30000	[62]
Microsized Sn	Ball-milling	1 M $NaPF_6$ in DGM	768/100	250	622/1690	[63]
Microsized Sn	Commercial	1 M $NaPF_6$ in PC + 5% FEC	>400/20	90	-	[65]
Microsized Sn	Electrodeposition	1 M $NaBF_4$ in EC/DMC	650/100	400	160/2000	[66]
μ-Sn	Commercial	1 M $NaPF_6$ in DGM + 0.01 M KPF_6	565/3000	2000	397.0/4000	[67]
μ-Sn	Commercial	1 M $NaPF_6$ in diglyme	455/2500	2000	450/4000	[68]
Bulk Sb	Ball-milling	1 M $NaClO_4$ in PC + 5% FEC	580/160	305	528/2440	[71]
Sb	Ball-milling	1 M $NaPF_6$ in EC/DEC + 5% FEC	500/>300	2000	440/4000	[73]
P–Sb	One step chemical steam dealloying	1 M $NaClO_4$ in PC + 5% FEC	413.6/120	50	300/3000	[74]
Sb PHMSs	Template	1 M $NaClO_4$ in PC + 5% FEC	617/100	100	312.9/3200	[75]
Micro-Sb/C@MXene	Hydrothermal	1 M $NaClO_4$ in EC/DEC + 5% FEC	407.1/100	100	191/10000	[76]
Black P	High-pressure and high-temperature	1 M $NaPF_6$ in EC/DEC + 1% VC	1587/24	125	1000/10000	[78]
P/G Hybrid	Ball-milling	1 M $NaClO_4$ in EC/DEC	>1700/60	260	520/526	[79]
Pb	Commercial	1 M $NaPF_6$ in diglyme	464/50	13	360/1950	[81]
Pb	Ball-milling	1 M $NaPF_6$ in DME	423/1000	4850	370/6208	[82]
Pb	-	1 M $NaPF_6$ in diglyme	464/50	13	360/2000	[83]
Ge	Magnetron sputtering	1 M $NaClO_4$ in PC + 5% FEC	>300/60	175	110/119000	[89]
Amorphous Ge	Acid etching	1 M $NaClO_4$ in EC/DEC	550/50	73.8	273/1845	[90]
Zn_3Sb_2	Pulse potential electrodeposition	1 M $NaClO_4$ in PC/EC + 5% FEC	263.9/320	300	308.7/1600	[91]
FeP_2	Ball-milling	1 M $NaPF_6$ in EC/DEC	955.1/30	89	900/3578	[92]
BiSn	Ultrasonic treatment at low temperature	1 M $NaPF_6$ in DGM	541/3000	2000	393/10000	[93]
Sn_4P_3/MWCNTs	Ball-milling	1 M $NaClO_4$ in FEC/DMC	452/120	100	259/1000	[94]

EC: ehtylene carbonate DEC: diethyl carbonate DME: ethylene glycol dimethyl ether PC: propylene carbonate DMC: Dodochem DGM: diethylene glycol dimethyl ether.

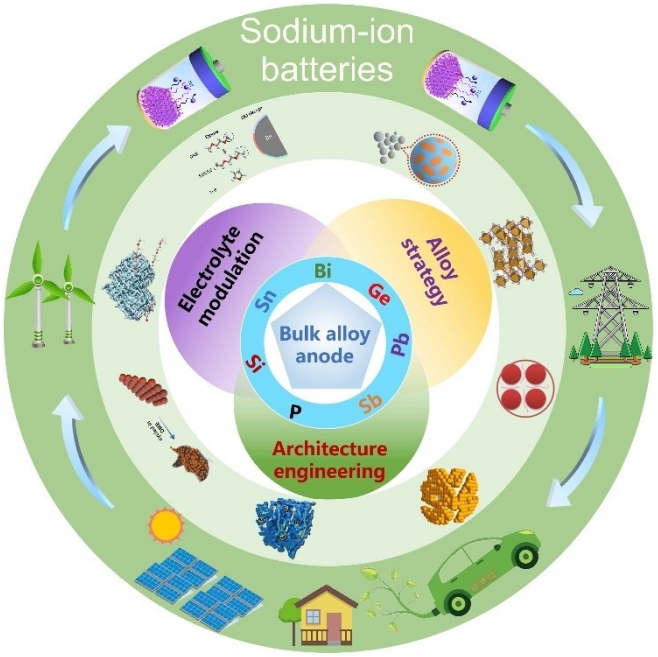

Figure 3. Modification strategies for bulk alloy anodes.

inexpensive resources.[54] Despite these advantages, challenges arise from the embedding and de-embedding of larger Na^+ during charge/discharge processes, causing significant volume expansion that can lead to crush of electrode and thus rapid capacity decay and poor rate performance. In the past, various approaches, such as electrolyte optimization and structural modifications, have been suggested to mitigate these issues and enhance the stability and performance of Bi anodes in SIBs.

Electrolyte is a critical component in SIBs, essential for charge balancing and transfer, as well as the formation and composition of SEI film. Careful selection of electrolyte is vital for stabilizing the electrode structure and forming a reliable SEI.[55] Wang et al. demonstrated enhanced Na storage performance by utilizing commercial bulk Bi paired with a $NaPF_6$-G2 electrolyte.[56] The bulk Bi gradually developed into a porous structure during initial cycling, aiding in minimizing strain and surface energy during reaction process with improved Na^+ transport kinetics (Figure 4a). Moreover, the solvent components of Na^+-G2 from the Bi electrode could permeate the bulk Bi's pores during cycling, preserving the porous structure and relieving the volume expansion (Figure 4b). Li et al. showed that solvated sodium in a diglyme-based electrolyte could alloy directly with Bi anode for sodium storage, achieving excellent electrochemical performance in a Bi//NVP@C full cell across a wide temperature range from −70 to 100 °C.[57] The Bi//NVP@C full cell with $NaPF_6$-G2 as electrolytes exhibited high power density (2354.6 $W\,kg^{-1}$) and energy density (150 $Wh\,kg^{-1}$).[58] Additionally, the electrolyte composition significantly influences the SEI film on the electrode surface. A suitable electrolyte can promote a stable SEI film, enhancing battery cycling and rate performance. Park's group analyzed the structure and chemical composition of SEI films on micron-sized Bi/C electrodes in ether and ester electrolytes using post mortem deep X-ray photoelectron spectroscopy and electron energy loss spectroscopy.[59] The study revealed that the multilayer SEI film formed in the ether electrolyte comprised a Bi-containing

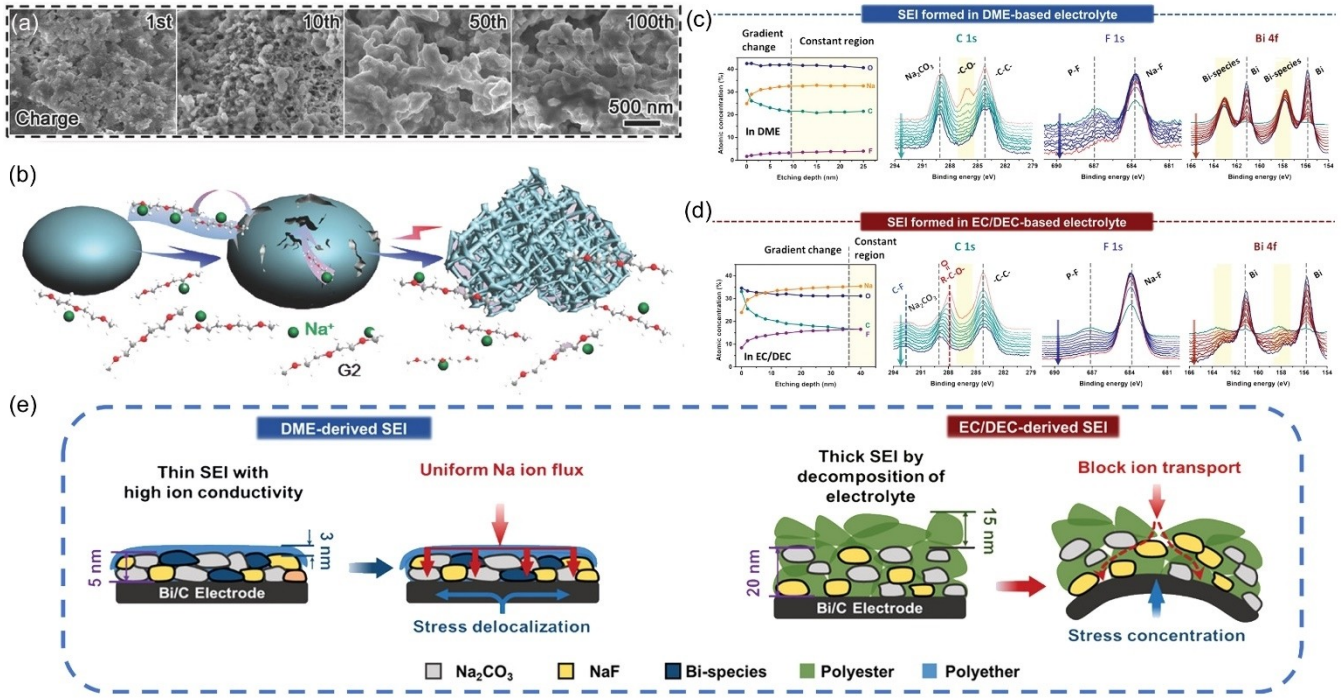

Figure 4. (a) SEM images of bulk Bi anode after cycles, (b) Schematic of the structural evolution of bulk Bi in G2 electrolyte with embedded/de-embedded Na. Reproduced with permission from Ref.[56] Copyright (2017) Wiley-VCH. (c) XPS analysis of bulk Bi alloy anode after 10 cycles in (c) DME and (d) EC/DEC electrolytes, (e) Structural diagram of Bi in DME and EC/DEC derived SEI. Reproduced with permission from Ref.[59] Copyright (2020) Wiley-VCH.

inorganic layer and a polyether-like outer layer (Figures 4c and d). In comparison to the SEI formed in the EC/DEC electrolyte, the SEI membrane in ether electrolyte was observed to be thinner yet possessed high mechanical strength and ionic conductivity, leading to enhanced cycling stability of the electrode (Figure 4e).

The development and synthesis of metallic Bi with a unique bulk phase structure have been shown to mitigate the volume expansion effects caused by the insertion and extraction of Na^+ during cycling. Guo et al. fabricated micrometer-scale porous Bi particles within carbon cages (P–Bi) as illustrated in Figure 5a.[60] The porous structure in bulk phases of P–Bi, characterized by continuous Bi pores (Figures 5b and c), serves as a buffer to accommodate volume changes during Na^+ embedding/de-embedding, resulting in high ICE (95.2%), exceptional cycling stability (20,000 cycles at a current density of 125 C), and enhanced capacity retention. Yu's group prepared self-healing nanostructured three-dimensional porous Bi (3DPBi) via a liquid-phase reduction approach, demonstrating through *in-situ* and *ex-situ* X-ray photoelectron spectroscopy (XPS) observations that the Bi continuous nanoporous network enables self-healing upon substantial volume fluctuations.[61] This property contributes to prolonged cycle life and enhanced capacity in both half-cells and full-cells utilizing 3DPBi as the anode. Furthermore, Zhang's group successfully fabricated FBi@NC anode materials by encapsulating flower-like micro-sized Bi particles within an elastic, nitrogen-doped carbon framework using a hydrothermal method (Figures 5e and f).[62] The interaction between Bi and N atoms in the FBi@NC structure facilitates Na^+ intercalation while preventing electrode material pulverization and detachment. Notably, the FBi@NC anode exhibits remarkable electrochemical performance in half-cells, maintaining 82.1% capacity retention after 10,000 cycles at 5 A g^{-1}. Strategies such as electrolyte optimization and tailored structural design have shown promise in advancing the practical utilization of bulk-phase metallic Bi, despite its relatively high mass leading to a lower theoretical specific capacity. Future efforts may focus on designing Bi-based alloys with multiple elements, such as Bi–Sn, Bi–Sn–Pb, and Bi–Sb, as an effective approach to further enhance their capacity and electrochemical properties.

2.2. Tin (Sn)

Sn is known for its non-toxicity, abundance, low cost and high electrical conductivity, making it highly valuable for high energy

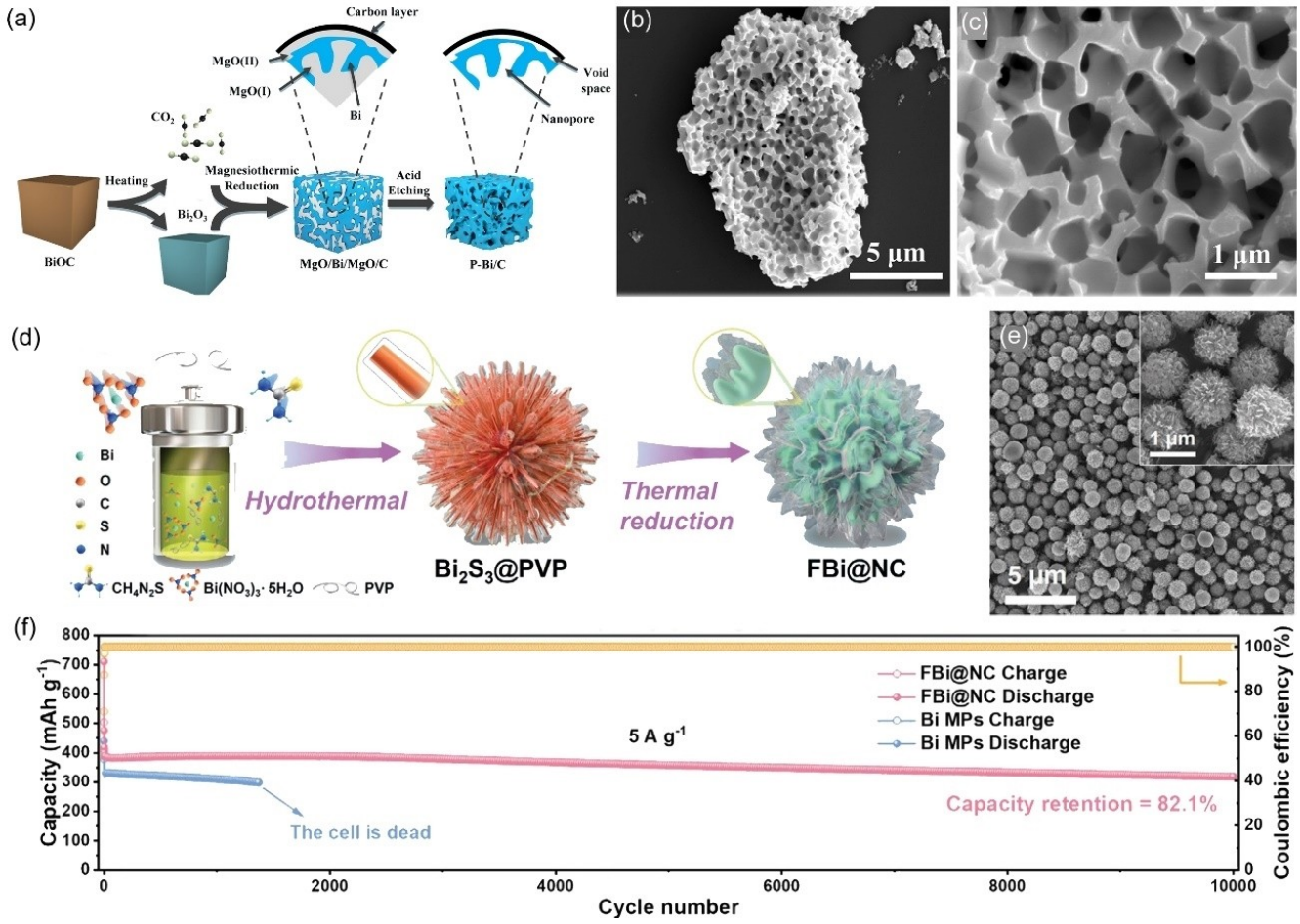

Figure 5. (a) Schematic of the synthesis process of P–Bi/C, (b, c) SEM images of P–Bi/C at different magnifications. Reproduced with permission from Ref.[60] Copyright (2023) Elsevier. (d) Preparation process and (e) SEM images of micrometer-scale FBi@NC (inset is at high magnification), (f) Cycling performance of FBi@NC at a current density of 5 A g^{-1}. Reproduced with permission from Ref.[62] Copyright (2024) Wiley-VCH.

storage. When alloyed with sodium, Sn can store 3.75 mol Na^+ to produce $Na_{15}Sn_4$, which shows a theoretical specific capacity of 847 mAh g^{-1}. The reversible sodiation/desodiation of Sn involves multiple phase transitions ($Sn \leftrightarrow NaSn_3 \leftrightarrow NaSn \leftrightarrow Na_9Sn_4 \leftrightarrow Na_{15}Sn_4$) resulting in four voltage platforms, as displayed in Figure 6a.[63,64] However, the large volume expansion (420%) during this process can cause pulverization and detachment of the electrode material, reducing cycling stability. To address these issues, strategies such as electrolyte optimization, electrolyte additives, and voltage regulation are being used.

Constructing a stable SEI film on the surface of metallic Sn anode materials through electrolyte optimization is an effective method to improve their electrochemical performance. Ether electrolytes are commonly used for Sn metal anode in SIBs. Researchers have extensively studied the electrochemical performance, composition of the SEI film, and solvation energy of these electrolytes. Amine's group found that micron-sized metallic Sn exhibits superior cycling stability and higher Coulombic efficiency in ether electrolytes when the SEIs formed have higher stability and mechanical strength (Figure 6b).[65] Additionally, Zhang's group reported a full SIB utilizing commercial bulk Sn as the anode and NVP as the cathode in an ether-based electrolyte exhibited high output voltage (~3.2 V) and high energy density (253.4 Wh kg^{-1}).[63] However, the detailed mechanism of Sn in ether electrolytes is not fully understood due to the complexity of the SEI structure and composition. Du et al. utilized XPS and nanoindentation techniques to analyze the structure and chemical composition of SEIs formed in ether and ester electrolytes with bulk Sn metal anodes.[64] The formation of SEI in ether-based electrolytes has been found to improve the mechanical properties of Sn, which is attributed to the dispersion of inorganic materials within a polymer-like matrix, resulting in enhanced cycling stability and rate performance. Research by Huang et al. revealed that the

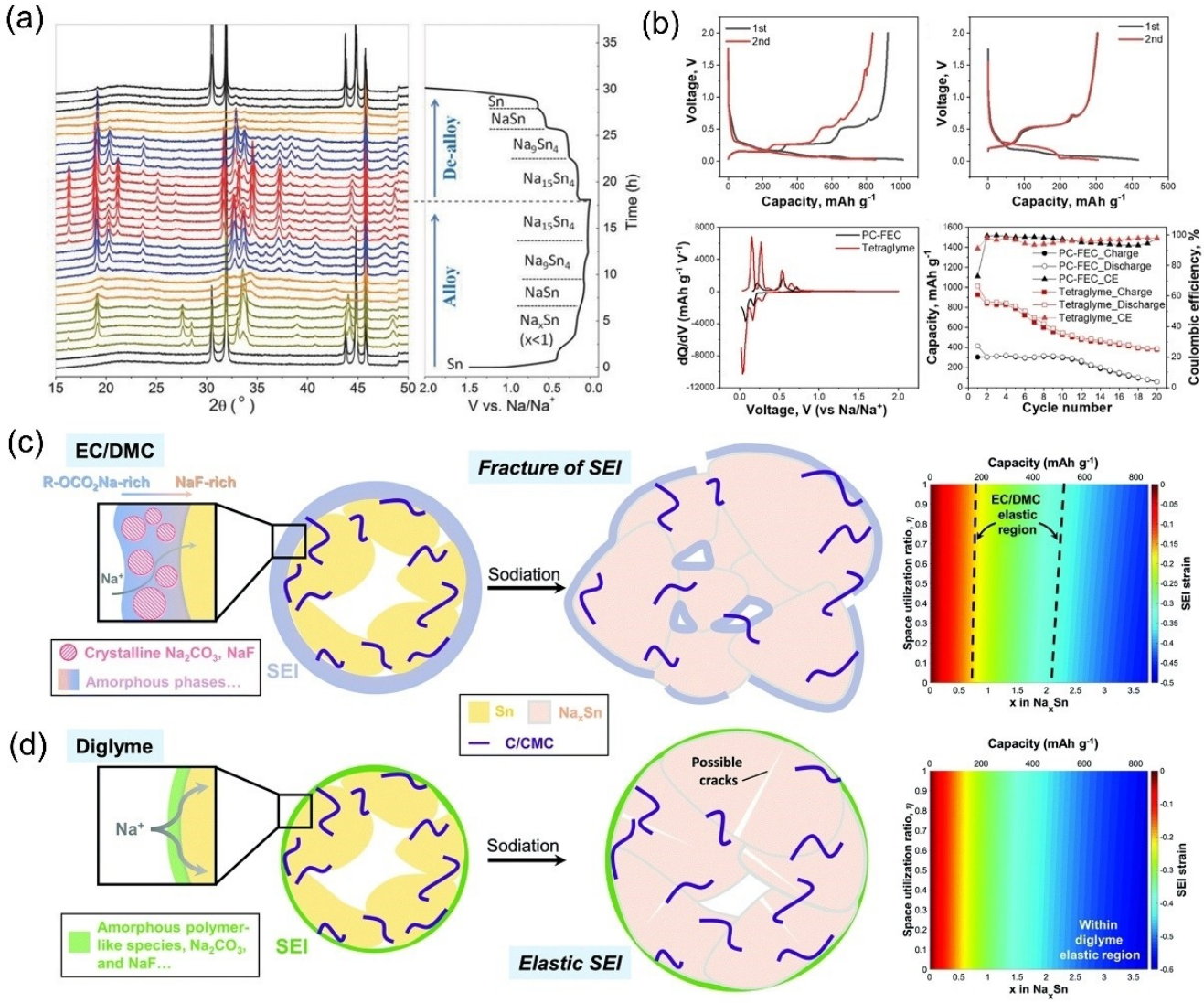

Figure 6. (a) *In-situ* XRD patterns of Sn in the first lap cycle. Reproduced with permission from Ref.[63] Copyright (2016) Wiley-VCH. (b) Electrochemical properties of micrometer-scale Sn anode in different electrolytes. Reproduced with permission from Ref.[65] Copyright (2023) Elsevier. Schematic representation of the composition and properties of SEI films of bulk phase Sn alloy anode in (c) $NaBF_4$/EC/DMC and (d) $NaBF_4$/diglyme electrolytes. Reproduced with permission from Ref.[66] Copyright (2019) Royal Society of Chemistry.

SEI formed on micrometer-sized Sn particles in ether electrolytes consists mainly of Na_2CO_3 and NaF, creating a thin and stiff polymeric layer (Figures 6c and d).[66] Additionally, Zheng et al. improved cycling stability and rate performance of Sn particles by incorporating K^+ as an electrolyte additive in ether electrolyte, providing electrostatic shielding.[67] This stabilized SEI film helps prevent electrolyte decomposition and surface-interface side reactions, mitigating volume expansion of the bulk Sn electrode during charging//discharging and improving its electrochemical performance. Zhu et al. also addressed the volume changes and structural stress in micron-particle Sn anodes by adjusting the voltage window.[68] These strategies are beneficial for the electrode structure and SEI stability of Sn bulk-phase electrodes, advancing their potential for commercialization.

2.3. Antimony (Sb)

Similar to Bi and Sn, metallic Sb as the anode material for SIBs, fully embedded Na^+ to generate Na_3Sb, has a specific capacity of up to 660 mAh g^{-1} along with a suitable working potential of around 0.45 V. Its pleated layered structure provides high density and excellent electrical conductivity (2.6×10^6 S m^{-1}).[69,70] However, during the alloying process with Na^+, Sb undergoes a significant volume expansion of up to 390% involving the formation of Na_3Sb, leading to electrode material crushing and detachment. To address this issue, researchers have employed strategies such as carbon composite integration, electrolyte optimization, and structural design improvements to enhance the electrochemical performance and safety of SIBs utilizing metallic Sb as the anode material.

In order to enhance the stability of the electrode-electrolyte interface, researchers have focused on regulating the electrolyte composition to construct a stable SEI film on the surface of the bulk phase Sb-metal anode electrode. Darwiche et al. successfully increased the stability of the Sb metal anode by incorporating 5% fluorinated ethylene carbonate (FEC) additive into the electrolyte.[71] The addition of FEC resulted in a 98% first cycle Coulombic efficiency and high cycling stability with a specific capacity of 525 mAh g^{-1} even after 50 cycles at 2 C current density ((Figures 7a and b). Similarly, Bian et al. observed the growth of a NaF-rich SEI film on the Sb electrode surface when 10% FEC additive was added to the electrolyte. This SEI film effectively prevented electrolyte decomposition, inhibited side reactions, and improved cycling stability.[72] Compared to the electrolyte without FEC additive, the Sb anode thickness slightly increased after 20 cycles in the presence of 10% FEC additive (Figures 7c and d), demonstrating its ability to effectively suppress electrolyte decomposition.

In addition to improving the electrochemical performance of Sb anode through electrolyte optimization, structural design, and the incorporation of carbon materials, there are other effective strategies that can be employed. Liu et al. utilized a controlled pre-deposition method of Sb with sodium biphenyl (Na–Bp) to selectively decompose the FEC electrolyte and create a NaF-rich SEI film on the metallic Sb electrode surface.

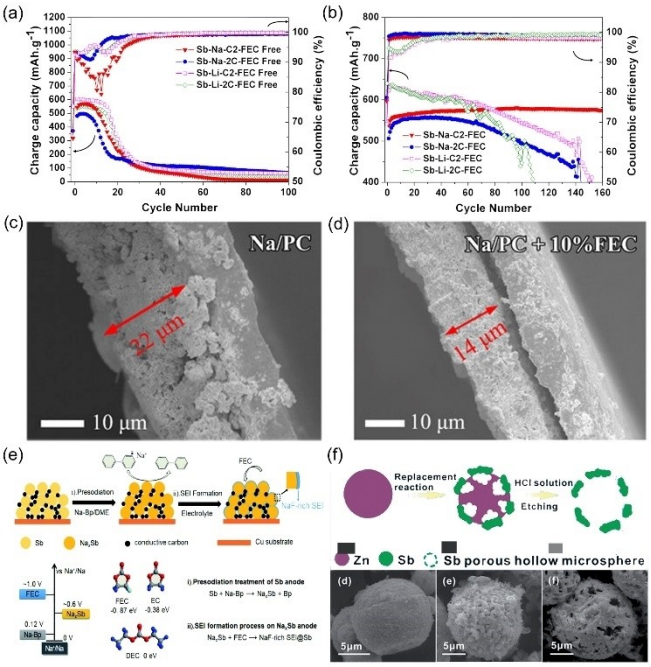

Figure 7. Cycling performance of micrometer-scale Sb alloy anode at different current densities with (a) addition of FEC and (b) no FEC additive. Reproduced with permission from Ref.[71] Copyright (2012) American Chemical Society. Cross-sectional SEM plots of Sb anode after cycling in (c) Na/PC and (d) Na/PC + 10% FEC electrolytes. Reproduced with permission from Ref.[72] Copyright (2020) American Chemical Society. (e) Schematic diagram of the insulation pretreatment process of Sb anode in Na–Bp/DME electrolyte. Reproduced with permission from Ref.[73] Copyright (2021) Royal Society of Chemistry. (f) Schematic of the synthesis process of Sb PHMSs and the corresponding SEM image. Reproduced with permission from Ref.[75] Copyright (2015) Royal Society of Chemistry.

This approach helped reduce electrolyte side reactions and mitigate the volume expansion of the Sb anode.[73] In addition, the full SIBs with NVP as cathode and Sb–pNa as anode exhibited high Coulombic efficiency (>95.0%) and a high energy density of 232 Wh kg^{-1} (Figure 7e). Gao's group developed Sb particles with a three-dimensional porous skeleton through a one-step chemical dealloying technique, which enabled them to be characterized by a high vibrational density of up to 2.33 g cm^{-2}, a small volume expansion and excellent electrochemical properties.[74] As shown in Figure 7f, Hou et al. used the template method to synthesize porous hollow microsphere Sb by substitution of Zn templates. Microsphere Sb anode showed excellent electrochemical performance in SIBs, with a reversible capacity of 617 mAh g^{-1} at 100 mA g^{-1} and high-capacity retention (97.2%).[75] Composite of Sb with carbon also improves its electrochemical properties. By encapsulating micron-sized metal particles of Sb in a carbon layer and $Ti_3C_2T_x$ MXene network, Cui's group has made a special structure with high electrical conductivity and elasticity, leading to a high volumetric capacity retention and a high rate performance (a volumetric capacity of 191.0 mAh cm^{-3} at 10 A g^{-1}).[76]

2.4. Phosphorus (P)

P can form an alloy with Na to create Na_3P alloy, offering a high theoretical specific capacity of 2596 mAh g^{-1} and a suitable operating voltage of approximately 0.45 V vs. Na^+/Na.[77] P exists in three natural: white, red, and black phosphorus. White P, with a tetrahedral configuration, is flammable and highly toxic. Red P, featuring a chain structure, exhibits high thermal stability and non-toxic properties but suffers from poor electrical conductivity (~1×10^{-12} S m^{-1}) and large volume expansion (~300%) after sodiation, leading to inadequate electrochemical stability. In contrast, black P, while possessing higher thermal stability and electrical conductivity (~1×10^{2} S m^{-1}) than white and red P, still exhibits subpar electrical conductivity. However, its complex preparation conditions render it unsuitable for large-scale synthesis. Due to its flammability, white P is unsuitable for use as an anode in SIBs. Consequently, extensive research has been conducted on red and black P to enhance their electrical conductivity, Na^+ diffusion kinetics, and reduce volume expansion, primarily through electrolyte optimization and carbon composite strategies.

Dahbi et al. effectively improved the electrochemical performance of black P powder anodes by introducing vinylene carbonate (VC) or fluoroethylene carbonate (FEC) additives to the electrolyte and forming a stable SEI film on the electrode-electrolyte interface (Figure 8a).[78] Analysis of the SEI composition through hard X-ray photoelectron spectroscopy (HAXPES) revealed the presence of inorganic compounds resulting from electrolyte and additive decomposition, offering a pathway to enhance the cycling stability and lifespan of black P anodes (Figure 8b). Enhancing the electrical conductivity of P can be achieved by creating a conductive network through its composite with carbon materials. Song et al. synthesized micrometer-particle phosphorus/graphene sheet hybrids (P/G) through a straightforward method, beneficial for enhancing conductivity, mitigating the large volume changes during Na^+ insertion/extraction, and improving SEI stability (Figures 8c and d).[79] The P/G hybrid anode demonstrates a notable reversible capacity of 1700 mAh g^{-1}, high Coulombic efficiency, and exceptional cycling stability over 60 cycles (Figure 8e). Despite advancements in the P anode, a comprehensive exploration of the reaction mechanism, structural changes, and SEI composition related to the encapsulated sodium is warranted for further understanding.

2.5. Other Elemental Alloys

Similar to Sn anode, metallic Pb undergoes full sodiation to form $Na_{15}Pb_4$, with a theoretical specific capacity of 485 mAh g^{-1}.[80] Pb exhibits promise for implementation in SIBs due to its high recovery rate of 99% from waste lead-acid batteries and cost-effectiveness. However, the hindrance of Pb in SIBs include its toxicity and substantial volume expansion rate of 375%. Researchers have addressed these challenges by enhancing electrochemical performance through strategies

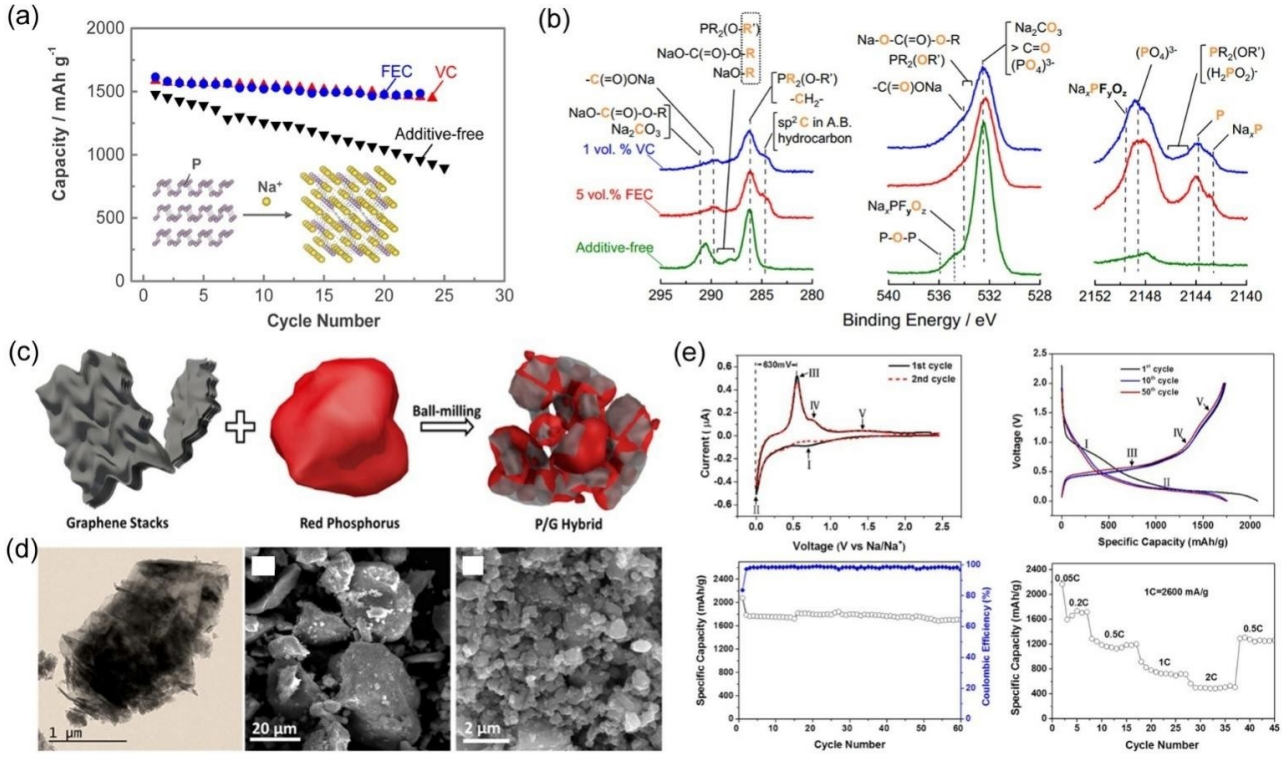

Figure 8. (a) Electrochemical performance of black P anodes with/without VC or FEC additives in the electrolyte, (b) HAXPES spectra of black P electrode after cycling in the additive-containing electrolyte. Reproduced with permission from Ref.[78] Copyright (2016) American Chemical Society. (c) Schematic of the synthesis process of P/G hybrid complex, (d) TEM and SEM images of P/G hybrid materials, (e) Electrochemical performance of the P/G electrode at 0–2 V. Reproduced with permission from Ref.[79] Copyright (2014) American Chemical Society.

such as electrolyte engineering and carbon compositing. For instance, Darwiche et al. developed highly loaded micron-sized Pb with notable capacity retention and minimal volume expansion in a 1 M $NaPF_6$ diethylene glycol electrolyte.[81] Similarly, Kim et al. fabricated micrometer-scale Pb metal anodes integrated with multi-walled carbon nanotubes to establish a robust conductive network, promoting efficient electron transport via ball milling.[82] The Pb anode electrode d exhibited prolonged cycling stability (maintaining a capacity of 423 $mAh\,g^{-1}$ after 1000 cycles at 10 C) and superior multiplicity performance in 1,2-dimethoxyethane electrolyte (DME). The full cell assembled by Pandit et al. with Pb as anode and NVP/C as cathode also showed excellent electrochemical performance (a capacity of 233 $mAh\,g^{-1}$ at 0.1 C).[83] Despite advancements in Pb anodes, a comprehensive exploration of their sodium storage mechanism and SEI composition remains lacking.

Si is a commonly utilized anode material in lithium-ion batteries due to its high capacity of 4200 $mAh\,g^{-1}$, forming $Li_{4.4}Si$ upon full alloying with Li^+.[84,85] However, when employed as an anode material in SIBs, Si undergoes an electrochemical alloying reaction with Na^+ to yield NaSi. Despite its high theoretical specific capacity of 954 $mAh\,g^{-1}$, Si exhibits a low reversible capacity ($<40\ mAh\,g^{-1}$) attributed to its inadequate electrical conductivity.[86–88] Strategies such as structural design and electrolyte modifications have been shown to improve the electrochemical performance of Si anodes. Ge has been investigated as an alternative anode material for SIBs, transforming into the amorphous phase NaGe upon full sodiation with a theoretical capacity of 369 $mAh\,g^{-1}$ and a volume expansion of 200%. Ge offers faster ion diffusion kinetics and superior electrical conductivity compared to Si, albeit still facing limitations in practical applications due to its electrical conductivity. Researchers have addressed these challenges through electrolyte optimization, structural modifications, and other approaches to enhance the development prospects of metallic Ge anodes in SIBs. For instance, the addition of FEC additives into propylene carbonate (PC) electrolytes has been demonstrated to form a stable SEI film on bulk Ge electrode surfaces, thereby enhancing electrochemical performance.[89] Synthesis of amorphous micro-sized Ge particles via acid etching of Mg_2Ge has also been investigated, resulting in an open porous channel structure facilitating Na^+ embedding/detachment and alleviating volume expansion issues.[90] These amorphous Ge anodes for SIBs have exhibited a high reversible capacity of 550 $mAh\,g^{-1}$, prolonged cycle life, and excellent rate capabilities. Despite recent advancements, the electrochemical properties and Na-storage mechanisms of Si and Ge anodes remain inadequately understood. Further exploration of the alloying mechanisms is imperative to enhance reversibility and realize the practical utilization of bulk Si and Ge anodes.

2.6. Multi-Component Alloys

In recent years, there has been significant research interest in multi-component alloys as anode materials for SIBs. These alloys typically consist of two or more elements and are categorized into electrochemically active-inactive and electrochemically active-active alloys. Electrochemically active elements, including Bi, Sn, Sb, Si, Ge, P, and Pb, are often combined with inactive elements such as Cu, Ni, Fe, Zn, etc. The incorporation of inactive elements into active metals serves to mitigate volume expansion, stabilize the material structure, and improve cycling stability. For instance, Shen et al. utilized pulse deposition to fabricate micro-sized Sb–Zn alloys on Cu foils, demonstrating enhanced stability, charge/discharge capacity, and cycle stability (Figures 9a and b).[91] Additionally, Manthiram et al. synthesized bulk-phase FeP_2 alloy, exhibiting a high charge/discharge capacity of 1137 $mAh\,g^{-1}$ and excellent cycling performance in SIBs, thus presenting a promising avenue for bulk-phase alloy anode development.[92] The introduction of inactive elements into alloy materials can alleviate the bulk effect, yet their non-alloying interaction with Na^+ diminishes the overall energy density of the electrode. Conversely, the introduction of electrochemically active elements facilitates the formation of intermetallic alloy compounds (e.g., Bi–Sn, Sn–Sb, etc.) that exhibit reactivity and can alloy with Na^+. The synergy among diverse metals plays a crucial role in adjusting the potential plateau, enhancing capacity, and increasing overall energy density. Furthermore, multiple element alloys comprising two or more electrochemically active elements have garnered significant attention from researchers due to their high specific capacity. For instance, Qian et al. fabricated micrometer-sized BiSn alloys through ultrasonic treatment of the molten metal, resulting in a homogeneous distribution of spherical Bi and Sn elements on the anode (Figures 9c and d).[93] This approach yielded a synergistic combination of Sn's high specific capacity and Bi's exceptional stability. Consequently, the BiSn alloy anode exhibited a notable reversible specific capacity of 607.2 $mAh\,g^{-1}$ and prolonged cycle life at a current density of 0.1 $A\,g^{-1}$, along with outstanding rate capability (achieving a capacity of 393 $mAh\,g^{-1}$ even at 10 $A\,g^{-1}$). Meanwhile, Mao et al. enhanced the cycling stability of Sn anodes by synthesizing Sn_4P_3 alloy, leveraging the alloying reaction of phosphorus to mend the cracks formed during Sn alloying. This mechanism effectively prevented the complete pulverization and detachment of the anode material during cycling (Figure 9e).[94] The multi-component alloying approach has witnessed significant advancements, with the potential for future exploration of multi-element alloys or high-entropy alloying strategies to harness synergistic interactions among individual metal elements across various platforms and stages, to mitigate volume expansion and enhance cycle stability.

3. Conclusions and Future Prospects

In this review, we present a comprehensive analysis of recent advancements in bulk-phase alloy anode materials for SIBs. These materials offer significant electrochemical benefits owing to their high specific capacity and initial Coulombic efficiency. However, the multi-electron transfer alloying/dealloying reaction mechanism in bulk alloy anodes results in substantial volume changes during the charging/discharging process,

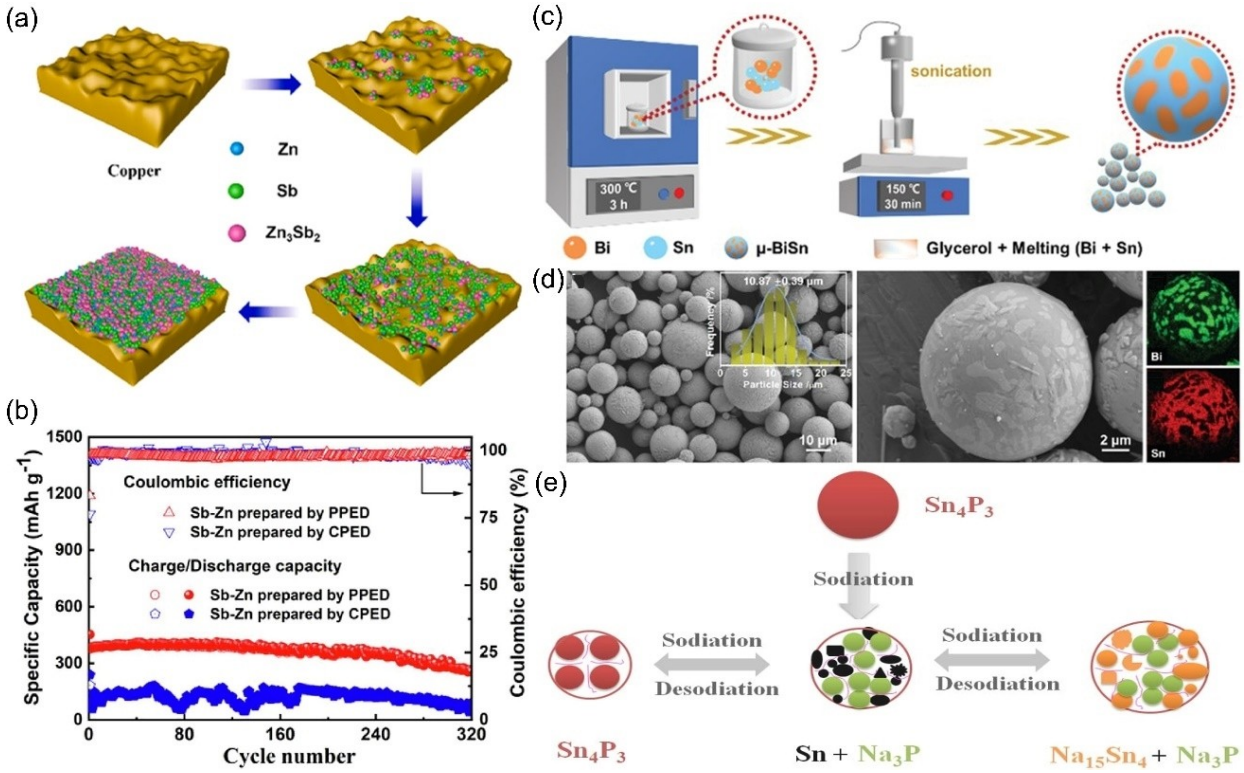

Figure 9. (a) Schematic synthesis of Zn_3Sb_2 on Cu foil using electrodeposition, (b) Cycling performance of Zn_3Sb_2 at 300 mA g^{-1}. Reproduced with permission from Ref.[91] Copyright (2023) Elsevier. (c) Schematic synthesis of micrometer-sized BiSn alloys, (d) SEM of BiSn alloys and the corresponding EDS plots. Reproduced with permission from Ref.[93] Copyright (2022) Royal Society of Chemistry. (e) Schematic structural evolution of Sn_4P_3 during charge and discharge processes. Reproduced with permission from Ref.[94] Copyright (2016) American Chemical Society.

leading to the detachment and deactivation of the electrode materials, causing fast capacity fading and hindering their practical application in SIBs. Overcoming these challenges is essential for the widespread adoption of bulk alloys in SIBs. Strategies such as mitigating volume expansion, enhancing conductivity, improving cycling stability and service life through carbon material composites, coating organic/inorganic conductive materials, employing special structural designs and optimizing electrolytes are crucial for advancing the utilization of bulk alloy anodes.

Despite significant advancements in bulk alloy anode materials, practical application still encounters challenges. These include minimizing volumetric energy density loss, relieving mechanical stress caused by the volume change, controlling volume expansion to prevent battery leakage, and enhancing initial Coulometric efficiency to prevent electrolyte decomposition. While progress has been made, bulk-phase alloy anodes for SIBs remain largely experimental in laboratory, hindering the development of high-performance full SIBs. Researchers acknowledge that optimizing electrolytes and electrode materials can greatly improve SIBs' electrochemical performance and safety. Exploring multi-element or high-entropy alloys is seen as a promising avenue for advancing bulk alloy anode materials and integrating them into large-scale energy storage systems. Continued research to design stable bulk alloy structures and compatible electrode-electrolyte systems is expected to lead to high-energy-density, long-lasting, and safe SIBs, facilitating their widespread use in energy storage applications.

Acknowledgements

This work was supported by the National Natural Science Foundation of China (22109037) and Multidisciplinary Research Project of Hebei University (DXK202309).

Conflict of Interests

The authors declare no conflict of interest.

Keywords: Sodium-ion batteries · Electrodes · Alloy anodes · Bulk structure · Energy storage

[1] S. Chu, Y. Cui, N. Liu, *Nat. Mater.* **2017**, *16*, 16.
[2] S. Li, K. Wang, G. Zhang, S. Li, Y. Xu, X. Zhang, X. Zhang, S. Zheng, X. Sun, Y. Ma, *Adv. Funct. Mater.* **2022**, *32*, 2200796.
[3] X. Zhou, Q. Liu, C. Jiang, B. Ji, X. Ji, Y. Tang, H. Cheng, *Angew. Chem. Int. Ed.* **2020**, *59*, 3802.
[4] Y. You, H. Yao, S. Xin, Y. Yin, T. Zuo, C. Yang, Y. Guo, Y. Cui, L. Wan, J. B. Goodenough, *Adv. Mater.* **2016**, *28*, 7243.
[5] C. Vaalma, D. Buchholz, M. Weil, S. Passerini, *Nat. Rev. Mater.* **2018**, *3*, 1.
[6] N. Yabuuchi, K. Kubota, M. Dahbi, S. Komaba, *Chem. Rev.* **2014**, *114*, 11636.

[7] E. Gabriel, C. Ma, K. Graff, A. Conrado, D. Hou, H. Xiong, *eScience* **2023**, *3*, 100139.
[8] C. Yang, S. Xin, L. Mai, Y. You, *Adv. Energy Mater.* **2021**, *11*, 2000974.
[9] C. Zhao, Q. Wang, Z. Yao, J. Wang, B. Sánchez-Lengeling, F. Ding, X. Qi, Y. Lu, X. Bai, B. Li, H. Li, A. Aspuru-Guzik, X. Huang, C. Delmas, M. Wagemaker, L. Chen, Y.-S. Hu, *Science* **2020**, *370*, 708.
[10] S. Guo, Q. Li, P. Liu, M. Chen, H. Zhou, *Nat. Commun.* **2017**, *8*, 135.
[11] C. Liu, K. Chen, H. Xiong, A. Zhao, H. Zhang, Q. Li, X. Ai, H. Yang, Y. Fang, Y. Cao, *eScience* **2024**, *4*, 100186.
[12] N. Liu, X. Zhao, B. Qin, D. Zhao, H. Dong, M. Qiu, L. Wang, *J. Mater. Chem. A* **2022**, *10*, 25168.
[13] V. Pamidi, C. Naranjo, S. Fuchs, H. Stein, T. Diemant, Y. Li, J. Biskupek, U. Kaiser, S. Dinda, A. Reupert, S. Behara, Y. Hu, S. Trivedi, A. R. Munnangi, P. Barpanda, M. Fichtner, *ACS Appl. Mater. Interfaces* **2024**, *16*, 25953.
[14] Q. Ni, Y. Bai, F. Wu, C. Wu, *Adv. Sci.* **2017**, *4*, 1600275.
[15] J. Peng, W. Zhang, Q. Liu, J. Wang, S. Chou, H. Liu, S. Dou, *Adv. Mater.* **2022**, *34*, 2108384.
[16] X. Zhao, N. Liu, M. Zheng, X. Wang, Y. Xu, J. Liu, F. Li, L. Wang, *ACS Energy Lett.* **2024**, *9*, 2748.
[17] L. Li, Y. Zheng, S. Zhang, J. Yang, Z. Shao, Z. Guo, *Energy Environ. Sci.* **2018**, *11*, 2310.
[18] S. Qiao, Q. Zhou, M. Ma, H. K. Liu, S. X. Dou, S. Chong, *ACS Nano* **2023**, *17*, 11220.
[19] X. Chen, Y. Zheng, W. Liu, C. Zhang, S. Li, J. Li, *Nanoscale* **2019**, *11*, 22196.
[20] D. Zhao, N. Zhang, X. Zhao, N. Liu, B. Qin, M. Qiu, L. Wang, *Sci. China Mater.* **2023**, *66*, 61.
[21] S. Huang, M. Wang, P. Jia, B. Wang, J. Zhang, Y. Zhao, *Energy Storage Mater.* **2019**, *20*, 225.
[22] L. Fang, N. Bahlawane, W. Sun, H. Pan, B. B. Xu, M. Yan, Y. Jiang, *Small* **2021**, *17*, 2101137.
[23] H. Hou, X. Qiu, W. Wei, Y. Zhang, X. Ji, *Adv. Energy Mater.* **2017**, *7*, 1602898.
[24] C. Chowdhury, S. Karmakar, A. Datta, *ACS Energy Lett.* **2016**, *1*, 253.
[25] T. Wang, K. Yao, Y. Hua, E. G. Shankar, R. Shanthappa, J. S. Yu, *Chem. Eng. J.* **2023**, *457*, 141363.
[26] Y. Fang, X.-Y. Yu, X. W. (David) Lou, *Adv. Mater.* **2018**, *30*, 1706668.
[27] S. Zhou, R. Jiang, S. Wang, L. Yu, X. Shi, L. Shao, Z. Sun, L. Hang, *J. Mater. Chem. A* **2024**, *12*, 11028.
[28] M. Lao, Y. Zhang, W. Luo, Q. Yan, W. Sun, S. X. Dou, *Adv. Mater.* **2017**, *29*, 1700622.
[29] H. Tan, D. Chen, X. Rui, Y. Yu, *Adv. Funct. Mater.* **2019**, *29*, 1808745.
[30] G. Yang, N. Li, C. Sun, *ACS Appl. Energy Mater.* **2020**, *3*, 12607.
[31] Z. Wang, Y. Mao, L. Sheng, C. Sun, *ACS Appl. Mater. Interfaces* **2024**, *16*, 12706.
[32] L. Wang, N. Liu, X. Zhao, X. Wang, T. Zhang, Z. Luo, F. Li, *Chem. Sci.* **2024**, *15*, 2133.
[33] C. Bommier, X. Ji, *Small* **2018**, *14*, 1703576.
[34] S. Liang, Y.-J. Cheng, J. Zhu, Y. Xia, *Small Methods* **2020**, *4*, 2000218.
[35] L. Yue, M. Jayapal, X. Cheng, T. Zhang, J. Chen, X. Ma, X. Dai, H. Lu, R. Guan, W. Zhang, *Appl. Surf. Sci.* **2020**, *512*, 145686.
[36] Y. Tian, Y. An, B. Zhang, *Adv. Energy Mater.* **2023**, *13*, 2300123.
[37] F. Li, Z. Zhou, *Small* **2018**, *14*, 1702961.
[38] D. Su, S. Dou, G. Wang, *Nano Energy* **2015**, *12*, 88.
[39] L. Wang, C. Wang, F. Li, F. Cheng, J. Chen, *Chem. Commun.* **2018**, *54*, 38.
[40] W. T. Jing, C. C. Yang, Q. Jiang, *J. Mater. Chem. A* **2020**, *8*, 2913.
[41] L. Wang, Y. Ni, K. Lei, H. Dong, S. Tian, F. Li, *ChemSusChem* **2018**, *11*, 3376.
[42] R. Shao, Z. Sun, L. Wang, J. Pan, L. Yi, Y. Zhang, J. Han, Z. Yao, J. Li, Z. Wen, S. Chen, S.-L. Chou, D.-L. Peng, Q. Zhang, *Angew. Chem. Int. Ed.* **2024**, *136*, e202320183.
[43] L. Shen, S. Shi, S. Roy, X. Yin, W. Liu, Y. Zhao, *Adv. Funct. Mater.* **2021**, *31*, 2006066.
[44] F. Yang, H. Gao, J. Chen, Z. Guo, *Small Methods* **2017**, *1*, 1700216.
[45] Y. Zhu, Y. Wen, X. Fan, T. Gao, F. Han, C. Luo, S.-C. Liou, C. Wang, *ACS Nano* **2015**, *9*, 3254.
[46] J. Eaves-Rathert, K. Moyer-Vanderburgh, K. Wolfe, M. Zohair, C. L. Pint, *Energy Storage Mater.* **2022**, *53*, 552.
[47] G. S. Reis, P. Molaiyan, C. M. Subramaniyam, F. García-Alvarado, A. Paolella, H. P. Oliveira, U. Lassi, *Electrochem. Commun.* **2023**, *153*, 107536.
[48] S. C. Jung, H. J. Kim, Y. J. Kang, Y. K. Han, *J. Alloys Compd.* **2016**, *688*, 158.
[49] H. Tan, D. Chen, X. Rui, Y. Yu, *Adv. Funct. Mater.* **2019**, *29*, 1808745.
[50] S.-M. Zheng, Y.-R. Tian, Y.-X. Liu, S. Wang, C.-Q. Hu, B. Wang, K.-M. Wang, *Rare Met.* **2021**, *40*, 272.
[51] L. Zhou, Z. Cao, W. Wahyudi, J. Zhang, J.-Y. Hwang, Y. Cheng, L. Wang, L. Cavallo, T. Anthopoulos, Y.-K. Sun, H. N. Alshareef, J. Ming, *ACS Energy Lett.* **2020**, *5*, 766.
[52] E. Edison, S. Sreejith, C. T. Lim, S. Madhavi, *Sustain. Energy Fuels* **2018**, *2*, 2567.
[53] S. Guo, Y. Feng, L. Wang, Y. Jiang, Y. Yu, X. Hu, *Small* **2021**, *17*, 2005248.
[54] L. Wang, A. A. Voskanyan, K. Y. Chan, B. Qin, F. Li, *ACS Appl. Energy Mater.* **2020**, *3*, 565.
[55] H. Che, S. Chen, Y. Xie, H. Wang, K. Amine, X. Liao, Z. Ma, *Energy Environ. Sci.* **2017**, *10*, 1075.
[56] C. Wang, L. Wang, F. Li, F. Cheng, J. Chen, *Adv. Mater.* **2017**, *29*, 1702212.
[57] Z. Li, Y. Zhang, J. Zhang, Y. Cao, J. Chen, H. Liu, Y. Wang, *Angew. Chem. Int. Ed.* **2022**, *61*, e202116930.
[58] C. Wang, D. Du, M. Song, Y. Wang, F. Li, *Adv. Energy Mater.* **2019**, *9*, 1900022.
[59] H. Yuan, F. Ma, X. Wei, J.-L. Lan, Y. Liu, Y. Yu, X. Yang, H. S. Park, *Adv. Energy Mater.* **2020**, *10*, 2001418.
[60] S. Guo, C. Wei, L. Wang, S. Mei, B. Xiang, Y. Zheng, X. Zhang, M. Javanbakht, B. Gao, P. K. Chu, K. Huo, *Cell Rep. Phys. Sci.* **2023**, *4*, 101463.
[61] X. Cheng, R. Shao, D. Li, H. Yang, Y. Wu, B. Wang, C. Sun, Y. Jiang, Q. Zhang, Y. Yu, *Adv. Funct. Mater.* **2021**, *31*, 2011264.
[62] Z. Chen, X. Wu, Z. Sun, J. Pan, J. Han, Y. Wang, H. Liu, Y. Shen, J. Li, D.-L. Peng, Q. Zhang, *Adv. Energy Mater.* **2024**, *14*, 2400132.
[63] B. Zhang, G. Rousse, D. Foix, R. Dugas, D. A. D. Corte, J.-M. Tarascon, *Adv. Mater.* **2016**, *28*, 9824.
[64] X. Du, Y. Gao, Z. Hou, X. Guo, Y. Zhu, B. Zhang, *ACS Appl. Energy Mater.* **2022**, *5*, 2252.
[65] A. Daali, X. Zhou, C. Zhao, I. Hwang, Z. Yang, Y. Liu, R. Amine, C.-J. Sun, W. Otieno, G.-L. Xu, K. Amine, *Nano Energy* **2023**, *115*, 108753.
[66] J. Huang, X. Guo, X. Du, X. Lin, J. Q. Huang, H. Tan, Y. Zhu, B. Zhang, *Energy Environ. Sci.* **2019**, *12*, 1550.
[67] C. Zheng, D. Ji, Q. Yao, Z. Bai, Y. Zhu, C. Nie, D. Liu, N. Wang, J. Yang, S. Dou, *Angew. Chem. Int. Ed.* **2023**, *62*, e202214258.
[68] Y. Zhu, Z. Qian, J. Song, W. Du, J. Pan, D. Wang, J. Yang, *Nano Lett.* **2021**, *21*, 3588.
[69] M. W. Orzech, F. Mazzali, J. D. McGettrick, C. Pleydell-Pearce, T. M. Watson, W. Voice, D. Jarvis, S. Margadonna, *J. Mater. Chem. A* **2017**, *5*, 23198.
[70] L. Wang, C. Wang, N. Zhang, F. Li, F. Cheng, J. Chen, *ACS Energy Lett.* **2017**, *2*, 256.
[71] A. Darwiche, C. Marino, M. T. Sougrati, B. Fraisse, L. Stievano, L. Monconduit, *J. Am. Chem. Soc.* **2012**, *134*, 20805.
[72] X. Bian, Y. Dong, D. Zhao, X. Ma, M. Qiu, J. Xu, L. Jiao, F. Cheng, N. Zhang, *ACS Appl. Mater. Interfaces* **2020**, *12*, 3554.
[73] M. Liu, Z. Yang, Y. Shen, S. Guo, J. Zhang, X. Ai, H. Yang, J. Qian, *J. Mater. Chem. A* **2021**, *9*, 5639.
[74] H. Zhang, W. An, H. Song, B. Xiang, S. Mei, Y. Hu, B. Gao, *Solid State Ion.* **2020**, *352*, 115365.
[75] H. Hou, M. Jing, Y. Yang, Y. Zhang, Y. Zhu, W. Song, X. Yanga, X. Ji, *J. Mater. Chem. A* **2015**, *3*, 2971.
[76] Y. Liang, Z. Wang, Z. Xu, S. Li, H. Luo, C. Xu, X. Cui, *Appl. Surf. Sci.* **2024**, *651*, 159234.
[77] J. Ni, L. Li, J. Lu, *ACS Energy Lett.* **2018**, *3*, 1137.
[78] M. Dahbi, N. Yabuuchi, M. Fukunishi, K. Kubota, K. Chihara, K. Tokiwa, X. Yu, H. Ushiyama, K. Yamashita, J.-Y. Son, Y.-T. Cui, H. Oji, S. Komaba, *Chem. Mater.* **2016**, *28*, 1625.
[79] J. Song, Z. Yu, M. L. Gordin, S. Hu, R. Yi, D. Tang, T. Walter, M. Regula, D. Choi, X. Li, A. Manivannan, D. Wang, *Nano Lett.* **2014**, *14*, 6329.
[80] X. Zhao, N. Liu, C. Mu, B. Qin, L. Wang, *J. Colloid Interface Sci.* **2024**, *669*, 647.
[81] A. Darwiche, R. Dugas, B. Fraisse, L. Monconduit, *J. Power Sources* **2016**, *304*, 1.
[82] C. Kim, H. Kim, M. K. Sadan, M. Jeon, G.-B. Cho, T.-H. Nam, K.-K. Cho, J.-H. Ahn, H.-J. Ahn, *J. Alloys Compd.* **2021**, *886*, 161240.
[83] B. Pandit, M. T. Sougrati, B. Fraisse, L. Monconduit, *Nano Energy* **2022**, *95*, 107010.
[84] H. Tian, X. Tan, F. Xin, C. Wang, W. Han, *Nano Energy* **2015**, *11*, 490.
[85] G. F. I. Toki, M. K. Hossain, W. U. Rehman, R. Z. A. Manj, L. Wang, J. Yang, *Ind. Chem. Mater.* **2024**, *2*, 226.
[86] D.-F. Qiu, X. Ma, J.-D. Zhang, Z.-X. Lin, B. Zhao, *Nanoscale Res. Lett.* **2018**, *13*, 275.

[87] M. Jiang, J. Chen, Y. Zhang, N. Song, W. Jiang, J. Yang, *Adv. Sci.* **2022**, *9*, 2203162.
[88] M. Jiang, J. Chen, H. Luo, Y. Ma, W. Jiang, G. Li, J. Yang, *Adv. Funct. Mater.* **2024**, *34*, 2316568.
[89] L. Baggetto, J. K. Keum, J. F. Browning, G. M. Veith, *Electrochem. Commun.* **2013**, *34*, 41.
[90] Z. Yi, N. Lin, T. Li, Y. Han, Y. Li, Y. Qian, *Nano Res.* **2019**, *12*, 1824.
[91] H.-R. Shen, X.-M. Zheng, Q.-L. Kang, P. Dai, X.-Y. Han, M.-G. Chen, B. Muniyandi, Q. Wu, G.-P. Tu, P.-Y. Zhang, R. Huang, L. Deng, J.-T. Li, L. Huang, S.-G. Sun, *Appl. Surf. Sci.* **2023**, *609*, 155243.
[92] W. Zhang, M. Dahbi, S. Amagasa, Y. Yamada, S. Komaba, *Electrochem. Commun.* **2016**, *69*, 11.
[93] Y. Zhu, C. Wang, Z. Cheng, Q. Yao, J. Su, B. Chen, J. Yang, Y. Qian, *Chem. Commun.* **2022**, *58*, 5140.
[94] J. Mao, X. Fan, C. Luo, C. Wang, *ACS Appl. Mater. Interfaces* **2016**, *8*, 7147.

Manuscript received: August 16, 2024
Revised manuscript received: September 19, 2024
Accepted manuscript online: September 24, 2024
Version of record online: October 31, 2024